

Timing Performance Study of New Fast PMTs With LYSO for Time-of-Flight PET

Mikiko Ito, Jin Pyo Lee, and Jae Sung Lee

Abstract—Most efforts at developing time-of-flight (TOF) positron emission tomography (PET) instruments have focused on improving their time resolution, which is affected by many factors. The aim of this study was to evaluate the performance of two new fast photomultiplier tubes (PMT) (Hamamatsu R9800 and R11194) for use as a TOF-PET detector, and to investigate the correlation of time resolution with time discrimination methods, the properties of the PMTs, the locations of the scintillation crystal on the PMT, and the size of the scintillation crystal. The PMTs evaluated in this study have fast rise time and short time jitter. The performance evaluation of the PMTs was conducted using a LYSO scintillation crystal. A ^{22}Na source was placed between the testing detector and a reference detector (with a time resolution of 200 ps), and data were acquired by using the coincidence trigger of the two detectors. To determine the optimal time discrimination method, time resolutions were obtained using a leading-edge discriminator (LED) with various thresholds and a constant-fraction discriminator (CFD) with various CFD delays. The effects on time resolution of PMT properties, the crystal position on the PMT, and the size of the crystal were observed. Based on the comparison of time resolutions obtained by various time discrimination setups, the optimal setup was determined to be CFD with 1.0 ns CFD delay. When these PMTs were coupled with 4 mm \times 4 mm \times 10 mm LYSO crystal and CFD with 1.0 ns delay was used for time discrimination, the average time resolution (FWHM) for 7 R9800 was 200.5 ps and for 7 R11194 was 227.8 ps. The average energy resolutions were 11.1% and 11.8%, respectively. Time resolutions at the edge of the PMT were degraded due to light collection loss and worse transit time jitter. Time resolutions were inversely proportional to the square root of the numbers of photoelectrons per pulse. The numbers of photoelectrons increased proportionately with the blue sensitivity of individual PMTs. Time resolutions have a distinct dependence as a function of the length and cross-section of the crystal. The new fast PMT coupled with LYSO crystals allow for the improvement of timing performance in TOF-PET detectors. The results of this study will be of value as a guideline for optimizing the TOF-PET detector design using the fast PMTs.

Index Terms—Fast PMT, Hamamatsu R11194, Hamamatsu R9800, LYSO, time of flight (TOF), time resolution.

I. INTRODUCTION

RECENTLY there has been a growing interest in the time-of-flight (TOF) positron emission tomography (PET) scanner, because the incorporation of the TOF technique

Manuscript received December 16, 2011; revised April 07, 2012; accepted May 22, 2012. Date of publication October 18, 2012; date of current version February 06, 2013. This work was supported by grants from the Atomic Energy R&D Program (2008-2003852, 2010-0026012) and the WCU Program (R32-10142) through the KOSEF funded by the Korean Ministry of Education, Science and Technology.

M. Ito is with the Department of Nuclear Medicine, Seoul National University, Seoul 110-744, Korea.

J. P. Lee is with the Department of Nuclear Engineering, Seoul National University, Seoul 110-744, Korea.

J. S. Lee is with the Nuclear Medicine, Biomedical Sciences and WCU Brain & Cognitive Sciences Departments, Institute of Radiation Medicine, Medical Research Center, and Interdisciplinary Programs in Radiation Applied Life Science Major, Seoul National University, Seoul 110-744, Korea (e-mail: jaes@snu.ac.kr).

Digital Object Identifier 10.1109/TNS.2012.2215342

into PET (current time resolution of ~ 500 ps) has demonstrated a significant improvement in image quality [1], [2]. The TOF information, which is the difference in the arrival times of the two annihilation gamma-rays, provides localization of the annihilation position on the line-of-response (LOR) [3]–[5]. This allows the use of a segment-of-response (SOR) instead of LOR in image reconstruction, and reduces the propagation of noise along the LOR in the reconstructed images. The reduction of noise can be equated with an increase in sensitivity [6]. Furthermore, the additional TOF information enables PET images to achieve high signal-to-noise ratio (SNR) and high contrast, or short scan times [1], [4], [7].

It can be theoretically calculated that the gain of the improvement by using TOF information is proportional to $D/\Delta x$ in sensitivity and $\sqrt{D/\Delta x}$ in SNR [6], [8], [9]; where D is the diameter of the patient, Δx is the position uncertainty of the SOR ($\Delta x = c \cdot \Delta t/2$), c is the speed of light, and Δt is the time resolution (FWHM). In addition, real clinical cases show that the gains with TOF are higher for larger patients. Therefore, the major effort in developing TOF-PET scanners has focused on improving their time resolution to increase the gains with TOF [10].

To enhance the time resolution at the PET detector level, it is important to utilize fast PMTs with fast scintillation crystals. For this reason, many studies have been conducted using PMTs that have fast rise times and short time jitters, coupled with LaBr3 or LSO scintillation crystals that have short decay times of the light pulse and high light yields [11]–[15].

In this study, we evaluated the performance of two new fast PMTs (Hamamatsu R9800 and R11194) with a LYSO scintillation crystal; it was reported that LYSO possesses similar scintillation properties and is a good alternative to LSO crystal [16]–[20]. The aim of this study was to evaluate the properties of the two fast PMTs with a LYSO crystal for TOF-PET detector. In addition, we investigated the dependencies of time resolution as a function of time discrimination setup, PMT properties, and scintillation crystal size. Understanding these relationships will help the decision to design TOF PET detectors in consideration of the trade-off between time resolution and other performance characteristics of a PET detector.

II. MATERIALS AND METHODS

A. Scintillation Detector

The Hamamatsu R9800 and R11194 PMTs are equipped with 7–8 dynodes, which is less than in general PMTs (10–12 dynodes), to reduce transit time and the transit time variation [21]. The dynodes have a linear focusing structure to decrease the difference in the path lengths for individual electrons through the PMT that cause transit time variation [21]. The R9800 PMT

TABLE I
THE MAIN PROPERTIES OF THE TYPICAL HAMAMATSU R9800
AND R11194 PMTs

PMT model	HAMAMATSU	
	R9800	R11194
Supply voltage	-1300V	-1300V
Rise time [ns]	1.0	1.2
Transit time [ns]	11	15
Transit time jitter (FWHM)[ps]	270	400
Gain	1.1×10^6	0.5×10^6
Photocathode	Bialkali	Bialkali
Blue sensitivity index	11	11
Peak wavelength [nm]	420	420
Dimension [mm]	Ø25	Ø38
Effective area [mm]	Ø22	Ø34
The number of dynode stages	8	8

in a cylindrical configuration has a diameter of 25 mm (1 inch) and the R11194 has a diameter of 38 mm (1.5 inches). The main properties of the PMTs are presented in Table I.

We initially conducted the performance evaluations of the fast PMTs using a LYSO crystal with a crystal size of 4 mm × 4 mm × 10 mm. We also investigated the effects of crystal size on detector performance as described later in Section II-E. All surfaces of the crystal were mechanically polished. The five surfaces except the one connecting to the PMT window were covered by two layers of ESR reflector that has 98% reflectivity and 0.065 mm thickness [22]. The crystal was optically coupled to the center of the fast PMTs with optical grease. The PMTs were operated at -1300 V and the output pulses of 511 keV level with 50 Ohm termination had approximately 350–400 mV amplitudes.

B. Scintillation Properties

For the measurement of the scintillation properties in the scintillation detector, the LYSO crystal was irradiated by using a ^{22}Na gamma source with 1.0 MBq activity. The PMT output pulses were connected to a digital phosphor oscilloscope (Tektronix MSO4034) with a 50 Ω termination, and sampled with 2.5 GS/s (350 MHz bandwidth, 1 ns rise time). Fig. 1 shows the average pulse shape of 1000 output signals for the R9800 and R11194 PMTs. The rise time was calculated from the time difference between 10% and 90% of the maximum amplitude. The decay time was obtained by the exponential fitting of the output decay pulse between 90% and 10% of the maximum amplitude.

C. Data Acquisition Setup

Data were acquired by using the coincidence trigger of two fast-PMT-based scintillation detectors (the testing detector and a reference detector) [23]. The reference detector also consists of the Hamamatsu R9800 PMT with a LYSO crystal (4 mm × 4 mm × 10 mm). Its time resolution (FWHM) was calculated to be 199.9 ps for the 511 keV energy peak. The calculation and result are described in more detail later.

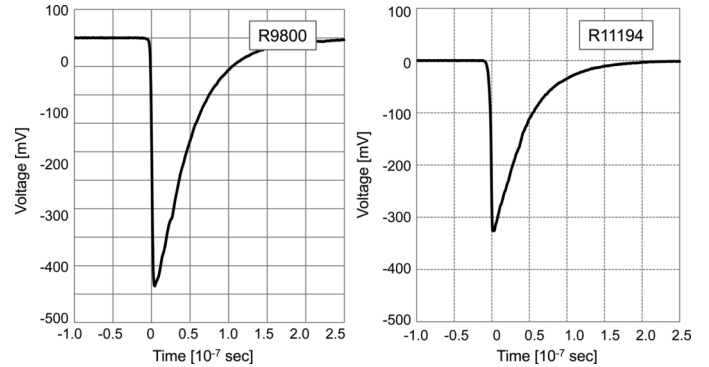


Fig. 1. Average output pulse shapes of the R9800 and P11194 PMTs with a $4 \times 4 \times 10$ mm LYSO crystal coupled at the center of PMT.

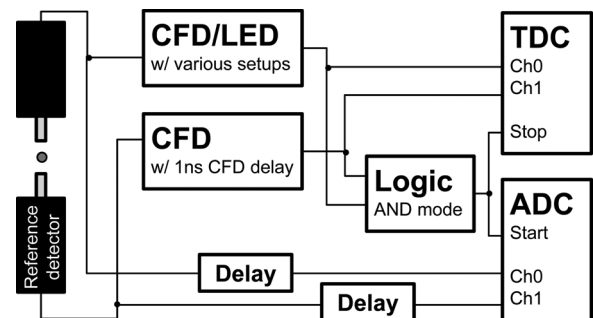


Fig. 2. Block diagram showing the experimental setup to acquire coincidence data.

Since timing performance is influenced by the timing discrimination setup, finding the optimal setup is important to obtain the best timing performance. To determine the optimal setup, time resolutions were measured by using various timing discrimination setups: a leading-edge discriminator (LED: CAEN N840) with various threshold voltages and a constant-fraction discriminator (CFD: ORTEC 935) with various CFD delay times.

As illustrated in Fig. 2, PMT anode signals were connected to the time discriminators (LED or CFD). Using the output signals (width of 20 ns) from the LED or CFD, the coincidence trigger signals were generated by a logic unit with AND mode (CAEN N455). The trigger signals were used for GATE signals of an analog-to-digital converter (ADC: CAEN V965) with a common start mode and a time-to-digital converter (TDC: CAEN V775N) with a common stop mode [24]. The width of the trigger signals (corresponding to the ADC integrating time) was adjusted to 200 ns in a GATE generator (CAEN N938).

By comparing the results, we determined the optimal time discrimination setup to provide the best time resolution. All performances of the fast PMTs were measured using the optimal setup.

Energy resolutions were calculated by the ratio of FWHM to mean value of the peaks corresponding to 511 keV photo-electron interactions in the energy distribution. Coincidence time resolutions were obtained by FWHM of the peaks in the time difference distribution for coincidence events of 450–570 keV in the energy distribution.

TABLE II
COINCIDENCE TIME RESOLUTION (FWHM) OF THE FAST PMTs WITH A LYSO CRYSTAL LOCATED AT THE CENTER OF THE PMT. DATA WERE MEASURED BY USING A CFD WITH A 1.0 NS CFD DELAY

Coincidence time resolution [ps]	R9800			
	PMT _a	PMT _b	PMT _c	PMT _d
PMT _a	-	-	-	-
PMT _b	286.6	-	-	-
PMT _c	278.2	282.4	-	-
PMT _d	279.6	280.6	279.8	-

D. Time Resolution of the Reference Detector

Coincidence time resolution ($FWHM_{a-b}$) involves both the time uncertainties ($FWHM_a$ and $FWHM_b$) of the two PMTs (PMT_a and PMT_b used for the coincidence measurements, as indicated in (1)).

$$FWHM_{a-b} = \sqrt{FWHM_a^2 + FWHM_b^2}. \quad (1)$$

To estimate the time resolution (FWHM) of the reference detector, four R9800 PMTs coupled with LYSO crystal were used. The coincidence time resolutions of all pairs using the four PMTs were measured by using the CFD with a 1 ns CFD delay, as presented in Table II.

$$\begin{pmatrix} 1 & 1 & 0 & 0 \\ 1 & 0 & 1 & 0 \\ 1 & 0 & 0 & 1 \\ 0 & 1 & 1 & 0 \\ 0 & 1 & 0 & 1 \\ 0 & 0 & 1 & 1 \end{pmatrix} \begin{pmatrix} FWHM_a^2 \\ FWHM_b^2 \\ FWHM_c^2 \\ FWHM_d^2 \end{pmatrix} = \begin{pmatrix} (286.6)^2 \\ (278.2)^2 \\ (279.6)^2 \\ (282.4)^2 \\ (280.6)^2 \\ (279.8)^2 \end{pmatrix}. \quad (2)$$

The individual time resolutions of the four PMTs were obtained by solving the linear equations in (2). The time resolution ($FWHM_a$) of the reference detector was estimated to be 199.9 ps.

E. The Correlation of Time Resolution With PMT Properties, Crystal Positions on PMT, and Crystal Size

The performance of 14 PMTs (7 R9800-PMTs and 7 R11194-PMTs) was measured with a LYSO crystal (4 mm × 4 mm × 10 mm) optically coupled to the center of the PMTs by using the optimal time discrimination setup. We investigated the correlation of time resolution with PMT properties such as blue sensitivity and gain.

The main properties of the individual PMTs are presented in Table III; Hamamatsu Photonics provided the properties of the individual PMTs, specifically, cathode sensitivity, anode sensitivity, blue sensitivity index, and dark current. PMT gains were calculated as the amplification ratio between cathode sensitivity and anode sensitivity. This gain includes the collection efficiency (ratio of collected number of photoelectrons by the first dynode compared to the emitted photoelectrons from photocathode, ~ 90%) compared with the pure gain calculation using a single photon pulse. The numbers of photoelectrons were estimated from the charge value of 511 keV photoelectric peaks divided by the PMT gain.

To observe PMT performance dependence on crystal positions in the PMT window, a LYSO crystal was optically coupled to five positions in the PMT window (the center and four edge positions on PMT surface) as shown in Fig. 8. The energy peak value, energy resolution, and time resolution were measured for the five positions.

Additionally, the effect of crystal size on time resolution was studied as a function of crystal cross-section (3 mm × 3 mm and 4 mm × 4 mm) and length (10, 20, and 30 mm). We tested 10 crystals in each size to consider the variation of crystal performance. In common with the above mentioned experimental setup, all surfaces of the LYSO crystals were mechanically polished and the five surfaces were wrapped with two layers of ESR reflector. The crystals were coupled to the center of the fast PMTs with optical grease.

III. RESULTS

A. Output Signal Pulse Property

The output pulses in Fig. 1 were averaged over 1000 acquisitions sampled by the oscilloscope. Based on the measurement of the shapes of the average output pulses, the rise time and decay time were estimated to be 2.92 ns and 41.9 ns for R9800, and 2.95 ns and 45.2 ns for R11194 PMT, respectively. These measured rise time would include the limitation of the scope bandwidth, the variations in pulse shape, and different arrival times of individual optical photons due to crystal geometry.

B. Time Resolution Dependence Against Time Discrimination Setup

Since the timing performance of the detectors was influenced by the time discrimination setup, finding the optimal setup was required to obtain the best time resolution of the PMTs.

Figs. 3(a) and 3(b) show the time resolutions (FWHM) obtained by using an LED with various thresholds (1, 3, 5, 10, 15, and 20% of pulse peak voltages) and using a CFD with various CFD delay times (0.0 to 3.5 ns at 0.5 ns intervals); the CFD delay times were set by adjusting the length of the external cable. The time resolutions (FWHM) were calibrated by the contribution of the time uncertainty of the reference detector. Based on the comparison of the results, the best time resolution was obtained when we used the CFD with a 1.0 ns CFD delay. As a result, the optimal time discrimination setup was determined to be the CFD with a 1.0 ns delay.

The time difference distributions of R9800 and R11194 as shown in Figs. 4(a) and 4(b) and energy distributions in Figs. 5(a) and 5(b) were measured in the optimal time discrimination setup. The time resolutions of 194.9 ps for R9800 and 223.7 ps for R11194 were obtained with a LYSO crystal (4 mm × 4 mm × 10 mm). Energy resolutions at 511 keV were 11.4% and 12.1%, respectively.

C. PMT Property Dependence

There are variations in the properties of individual PMTs for 7 R9800 and 7 R11194 PMTs, as indicated in Table II. The tested R9800 PMTs have a higher blue sensitivity (12.0 ~ 12.4) than the typical blue sensitivity in Table I. We studied the performance dependence on the properties of individual PMTs. En-

TABLE III
THE PROPERTIES OF THE INDIVIDUAL PMTs MEASURED WITH OVERALL SUPPLY VOLTAGE OF -1300 V.
INFORMATION WAS PROVIDED BY THE MANUFACTURER (HAMAMATSU PHOTONICS)

PMT model		Cathode sensitivity [μ A/lm]	Anode sensitivity [A/lm]	PMT gain [$\times 10^6$]	Blue sensitivity [μ A/lm_b]	Anode dark current [nA]
R9800	PMT ₁	129	119	0.922	12.1	0.74
	PMT ₂	148	129	0.872	12.4	2.7
	PMT ₃	151	176	1.17	12.4	15
	PMT ₄	148	131	0.885	12.2	7.8
	PMT ₅	142	123	0.866	12.0	1.5
	PMT ₆	143	91.3	0.638	12.2	0.74
	PMT ₇	140	138	0.986	12.1	8.3
R11194	PMT ₁	88.5	121	1.37	11.0	2.3
	PMT ₂	80.6	113	1.40	10.5	2.5
	PMT ₃	92.8	37.6	0.405	10.5	0.85
	PMT ₄	86.3	32	0.371	10.3	1.1
	PMT ₅	114	46.7	0.410	11.6	0.91
	PMT ₆	117	44.8	0.383	11.5	1.5
	PMT ₇	86.3	32.7	0.379	10.6	1.1

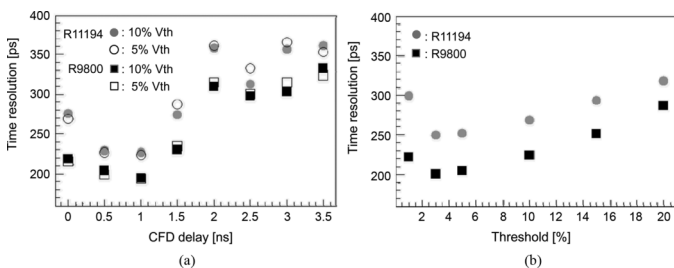


Fig. 3. Time resolution dependence against the time discrimination setup in electronics. (a) Single timing resolutions (FWHM) measured by using a LED with various threshold voltages (1, 3, 5, 10, 15, 20% of pulse amplitudes) and (b) Using a CFD with various CFD delay times (0–3.5 ns at 0.5 ns intervals).

ergy and time distributions of each PMT were measured by using a LYSO crystal (4 mm \times 4 mm \times 10 mm) coupled at the center of the PMT.

The average time resolution (FWHM) for 7 R9800 PMTs was 200.5 ps and for 7 R11194 PMTs was 227.8 ps. The average energy resolutions were 11.1% and 11.8%, respectively.

Fig. 6(a) shows the correlation between blue sensitivity and the number of photoelectrons calculated from the charge value of the energy peak calibrated by the gain. Fig. 6(b) is indicative of the $1/\sqrt{N_{\text{phe}}}$ dependence on time resolution. The time resolutions in Fig. 6(b) were inversely proportional to the square root of N_{phe} per pulse. The numbers of photoelectrons increased proportionately with the blue sensitivity of the individual PMTs, as shown in Fig. 6(a). These results indicated that the timing performance of the PMTs correlates with the blue sensitivity of the PMTs.

To observe the time resolution dependence on the gain of the PMT, the energy peak values and time resolutions in Fig. 7 were measured with various supply voltages (-1200 – -1400 V). PMT gain increased constantly with the supply voltage, while the time resolutions showed no significant change against the supply voltages.

D. Crystal Position Dependence

Measurements of PMT output pulse, energy resolution, and time resolution (FWHM) were conducted for the five crystal positions over the PMT entrance window as illustrated in Fig. 8. Table IV summarizes the PMT output pulse, energy resolution, and time resolution for the five crystal positions of the PMTs; the output pulse (%) was normalized by the output pulse at the center of the PMT.

At the corner of the PMT, output pulse decreased by light collection loss due to the location dependence of blue sensitivity and photoelectron collection efficiency to the first dynode. The central region of the PMTs had the highest response, and provided the best timing performance.

E. Crystal Size Dependence

To investigate the effect of crystal size on timing performance, we measured PMT performance using various sizes of LYSO crystals as shown in Fig. 9: six pairs of two cross-section sizes (3 mm \times 3 mm and 4 mm \times 4 mm) and three crystal lengths (10, 20, and 30 mm).

Figs. 10(a) and 10(b) show PMT output, which is proportional to the light pulse, and timing measurements as a function of crystal length and cross-section, respectively. In Fig. 10, the data points indicate the average value of the performances over ten LYSO crystals in each size shown in Fig. 9, and the error bars indicate the standard deviation of the data.

The result in Fig. 10(a) shows that light pulse decreased with increasing crystal length and decreasing cross-section because of the increased scatter and absorption of optical photons on the surface of reflector and increased self-absorption of photons within the crystal. In Fig. 10(b), the timing performance degraded due to the decreased light pulse, as mentioned in Section III-C. Especially for long crystals, additional time degradation was caused by different DOI positions and different optical transit time of scattered optical photons [25].

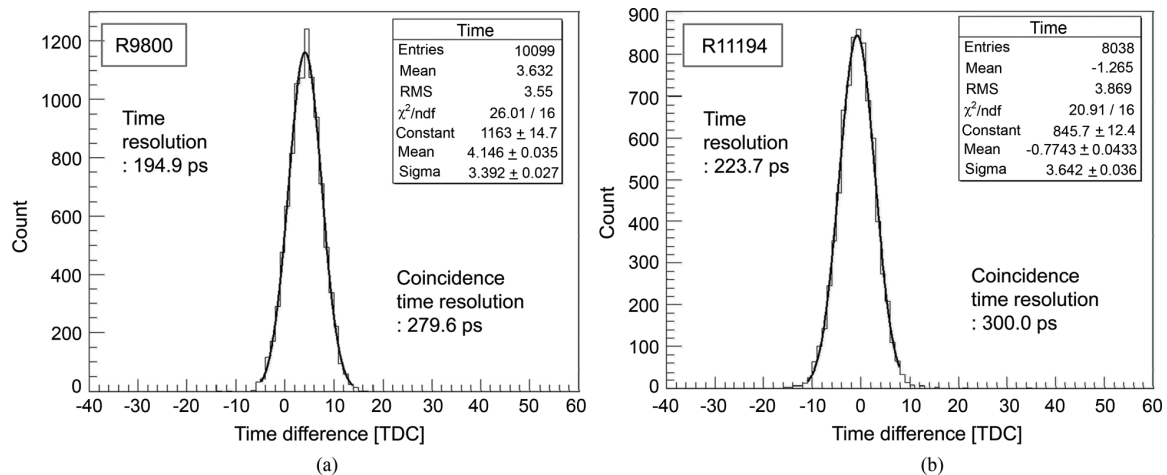


Fig. 4. Timing performance measured by fast PMTs with a LYSO crystal ($4 \times 4 \times 10$ mm) in the optimal time discrimination setup. Coincidence time difference distributions were obtained by using (a) R9800 and (b) R11194 PMTs.

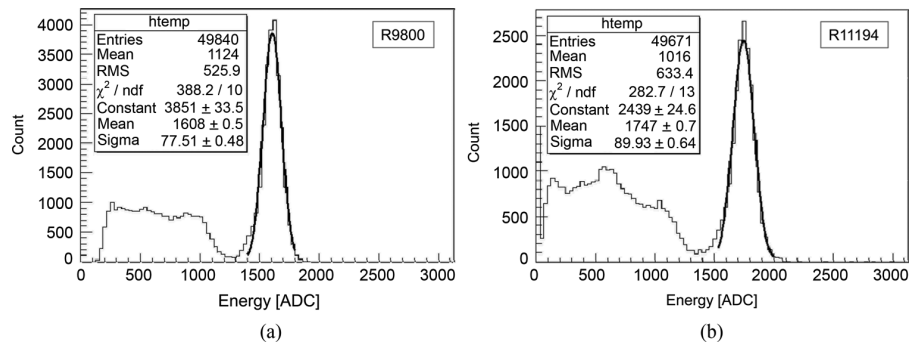


Fig. 5. Energy performance measured by fast PMTs with a LYSO crystal ($4 \times 4 \times 10$ mm) in the optimal time discrimination setup. Energy distributions were obtained by using (a) R9800 and (b) R11194 PMTs.

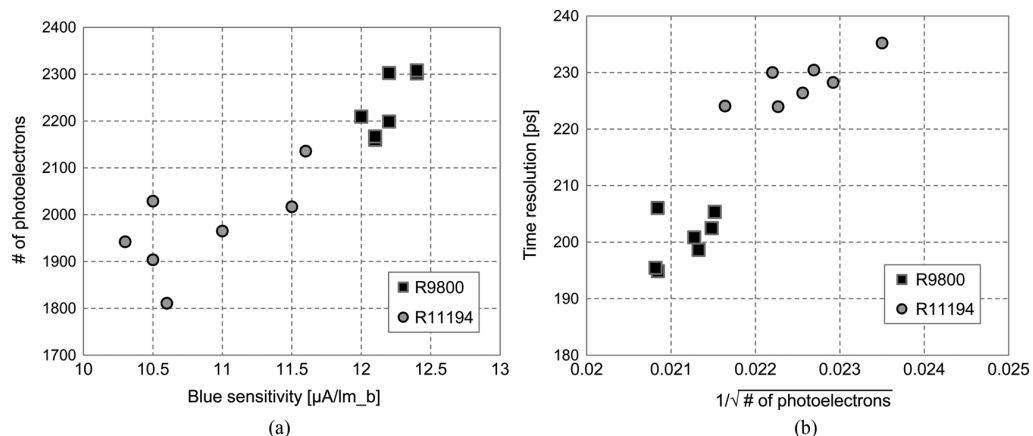


Fig. 6. The effect of the number of photoelectrons, and the blue sensitivity of individual PMTs on the time resolution (a) The number of photoelectrons emitted from the photocathode in the PMT against the blue sensitivity of the individual PMTs and (b) The correlation of time resolution with the number of photoelectrons.

IV. DISCUSSION

It is well recognized that the timing performance of PET detectors is affected by several factors. Therefore, the factors influencing time resolution have been studied by Monte Carlo simulations and experiments for an optimization of all factors in TOF-PET detectors [26]–[28]. In this study, we also investigated the effect of time discrimination setup, PMT properties, and scintillation crystal size on the time resolution of the new fast PMTs with a LYSO crystal.

Although we determined the optimal time discrimination setup to obtain the best timing performance by adjusting the

parameters of LED and CFD, the theoretical estimation of optimal setup has been also suggested. The time resolution using LED can be calculated by Hyman theory [29]. In the theory, the time resolution is estimated as a function of the number of photoelectrons, the decay constant of the light pulse, the time jitter of the PMT and its response for the single photoelectron. Then 1% threshold was suggested to be used for a fast PMT, and 4 ~ 7% for general PMTs [30]. In our experimental setup, however, the time resolutions obtained with 1% threshold were degraded due to higher signal noise level than the threshold level.

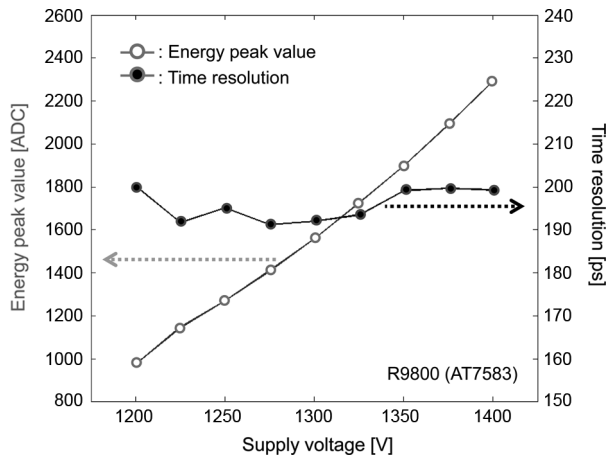


Fig. 7. Time resolution dependence on the gain of the PMT. Energy peak value (red circle point) and time resolution (blue square point) against the supply voltage.

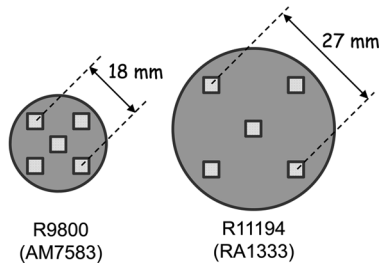
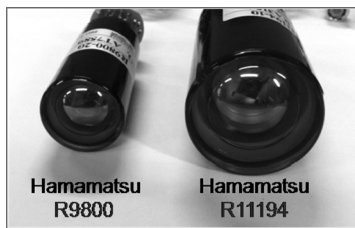


Fig. 8. The five positions of the LYSO crystal ($4 \times 4 \times 10$ mm) on the PMT entrance window for the measurement of the performance dependence on the crystal location; the center and four corner positions of the PMT window.

For CFD, it has been suggested that CFD delay time should be equal or less than the rise time of the pulse. An appropriate delay time is suggested as follows [31]:

$$\text{Delay time} = \text{rise time} \times (1 - \text{CFD fraction}).$$

where, the CFD fraction of our setup was 20%. The rise times measured by oscilloscope were about 2.9 ns for R9800 and R11194 PMTs. However, the output pulse in oscilloscope would include the several limitation factors mentioned in Section III-A. The actual rise time of PMT output pulse would be < 1.3 ns because LYSO has intrinsic rise time of < 200 ps and PMT rise time is 1.0 ns for R9800 and 1.2 ns for R11194. Therefore, the appropriate delay time calculated from above equation is approximately in a good agreement with the optimal CFD delay time of 1.0 ns obtained experimentally.

The results in Fig. 6(b) showed that the number of photoelectrons created at the photocathode of the PMT is a significant factor for timing performance, because the resolution is

TABLE IV
PERFORMANCE DEPENDENCE ON THE LOCATION OF THE LYSO CRYSTAL ON THE PMT WINDOW

PMT model	Location	Output pulse [%]	Energy resolution	Time resolution
R9800	Center	100	11.9%	209.5 ps
	Edge-1	94	12.0%	226.0 ps
	Edge-2	87	11.3%	242.6 ps
	Edge-3	86	11.4%	239.2 ps
	Edge-4	91	11.3%	230.6 ps
R11194	Center	100	12.1%	226.4 ps
	Edge-1	86	13.0%	247.0 ps
	Edge-2	79	12.4%	273.8 ps
	Edge-3	84	12.4%	265.1 ps
	Edge-4	94	12.1%	240.3 ps

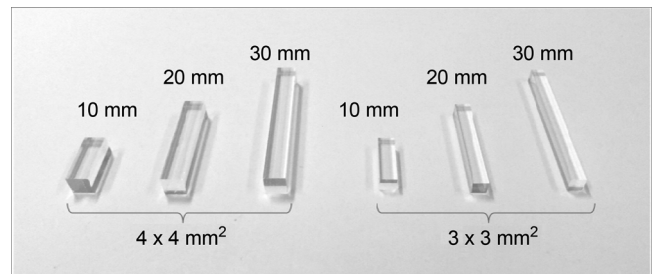


Fig. 9. Various sizes of LYSO crystals used in this study, all surfaces of which were mechanically polished.

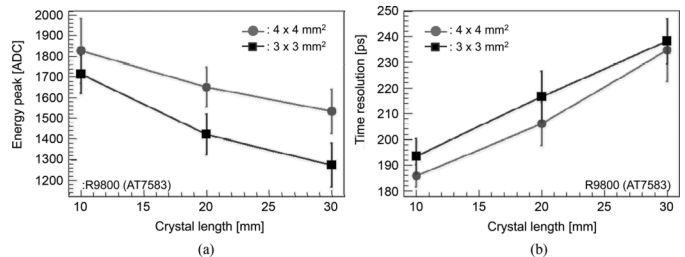


Fig. 10. (a) Light output and (b) Time resolution as a function of the crystal length and cross-section.

inversely proportional to the square root of the number of photoelectrons per pulse. This result is in good agreement with those of other investigations [12], [26], [30], [32]–[34]. The number of photoelectrons correlates with the blue sensitivity of the PMT (Fig. 6(a)), such that the blue sensitivity is the most important property of a PMT for the design of TOF-PET detectors.

Transit time jitter is also an important factor influencing the time resolution. Transit time jitter dependence of the timing performance has been investigated using various kinds of PMTs [35]. The results showed that time resolutions normalized to the number of photoelectrons were constantly degraded with the increase of time jitter. Although we have not measured the position dependency of transit time jitter of PMT, the worse timing resolution on the edge of PMT window than center would be also attributed to the worse transit time jitter at the periphery of PMT.

It is also well-known that timing performance is influenced by the scintillation crystal geometry that determines the pathway of light transport in the crystal and the arrival time dispersion of individual scintillation photons on the PMT surface [25], [36]. Moses and Derenzo reported that coincidence time resolution was degraded as the length of crystals increased, from 300 ps for two 3 mm × 3 mm × 3 mm LSO crystals to 475 ps for two 3 mm × 3 mm × 30 mm LSO coupled to a Hamamatsu R-5320 PMT [13].

As shown in Fig. 10, time resolution had a strong dependence on the crystal length and cross-section. The photoelectric peaks of 511 keV gamma rays in the energy distribution were decreased with increasing crystal length and with decreasing crystal cross-section, as shown in Fig. 10(a). It appears that light attenuation and collection loss were caused by multiple reflections. The degradation of timing performance indicated in Fig. 10(b) could be caused by a difference in the transport time between events with different depths of interaction (DOI) and time dispersion due to multiple reflection, besides the decrease in light output [13], [37].

The interaction of the factors influencing the time resolution is estimated to be summed in quadrature by assuming that most of these effects are independent [38].

V. CONCLUSION

In this study, a performance evaluation was conducted of two new fast PMTs, the Hamamatsu R9800 and R11194, coupled with a LYSO crystal. The results of this study demonstrated that excellent energy and time resolution performance could be obtained: when these PMTs were coupled with 4 mm × 4 mm × 10 mm LYSO crystal and CFD with 1.0 ns delay was used for time discrimination, the average time resolution (FWHM) for R9800 was 200.5 ps and for R11194 was 227.8 ps. The average energy resolutions were 11.1% and 11.8%, respectively. We conclude that these fast PMTs with LYSO allows for the improvement of timing performance in TOF-PET detectors.

Additionally, we investigated the effects of time discrimination setup, PMT properties, crystal positions, and crystal size on timing performance. The results of this study will be useful for guiding the optimization of the TOF-PET detector design using the fast PMTs and LYSO scintillation crystals.

REFERENCES

- [1] D. J. Kadrmas, M. E. Casey, M. Conti, B. W. Jakoby, C. Lois, and D. W. Townsend, "Impact of time-of-flight on PET tumor detection," *J. Nucl. Med.*, vol. 50, no. 8, pp. 1315–1323, 2009.
- [2] S. Surti, A. Kuhn, M. E. Werner, A. E. Perkins, J. Kolthammer, and J. S. Karp, "Performance of philips gemini TF PET/CT scanner with special consideration for its time-of-flight imaging capabilities," *J. Nucl. Med.*, vol. 48, no. 3, pp. 471–480, 2007.
- [3] R. Allemand, C. Gresset, and J. Vacher, "Potential advantages of a cesium fluoride scintillator for a time-of-flight positron camera," *J. Nucl. Med.*, vol. 21, no. 2, pp. 153–155, 1980.
- [4] N. A. Mullani, D. C. Ficke, R. Hartz, J. Markham, and G. Wong, "System-design of fast PET scanners utilizing time-of-flight," *IEEE Trans. Nucl. Sci.*, vol. NS-28, no. 1, pp. 104–107, 1981.
- [5] N. A. Mullani, J. Markham, and M. M. Terpogossian, "Feasibility of time-of-flight reconstruction in positron emission tomography," *J. Nucl. Med.*, vol. 21, no. 11, pp. 1095–1097, 1980.
- [6] J. S. Karp, S. Surti, M. E. Daube-Witherspoon, and G. Muehlechner, "Benefit of time-of-flight in PET: Experimental and clinical results," *J. Nucl. Med.*, vol. 49, no. 3, pp. 462–470, 2008.
- [7] M. Conti, B. Bendriem, M. Casey, M. Chen, F. Kehren, C. Michel, and V. Panin, "First experimental results of time-of-flight reconstruction on an LSO PET scanner," *Phys. Med. Biol.*, vol. 50, no. 19, pp. 4507–4526, 2005.
- [8] D. L. Snyder, L. J. Thomas, and M. M. Terpogossian, "A mathematical-model for positron-emission tomography systems having time-of-flight measurements," *IEEE Trans. Nucl. Sci.*, vol. NS-28, no. 3, pp. 3575–3583, 1981.
- [9] T. F. Budinger, "Time-of-flight positron emission tomography: Status relative to conventional PET," *J. Nucl. Med.*, vol. 24, no. 1, pp. 73–78, 1983.
- [10] J. S. Lee, "Technical advances in current PET and hybrid imaging systems," *Open Nucl. Med. J.*, vol. 2, pp. 192–208, 2010.
- [11] M. Moszynski, M. Kapusta, D. Wolski, M. Balcerzyk, S. O. Flyckt, P. Lavoute, C. Mannonier, and H. Mach, "New fast photomultipliers with a screening grid at the anode," *IEEE Trans. Nucl. Sci.*, vol. 51, no. 4, pp. 1701–1706, Aug. 2004.
- [12] M. Moszynska, M. Gierlik, M. Kapusta, A. Nassalski, T. Szczesniak, Ch. Fontaine, and P. Lavoute, "New photonic XP20D0 photomultiplier for fast timing in nuclear medicine," *Nucl. Instrum. Methods Phys. Res. A*, vol. 567, no. 1, pp. 31–35, 2006.
- [13] W. W. Moses and S. E. Derenzo, "Prospects for time-of-flight PET using LSO scintillator," *IEEE Trans. Nucl. Sci.*, vol. 46, no. 3, pp. 474–478, Jun. 1999.
- [14] A. Kuhn, S. Surti, J. S. Karp, G. Muehlechner, F. M. Newcomer, and R. VanBerg, "Performance assessment of pixelated LaBr3 detector modules for time-of-flight PET," *IEEE Trans. Nucl. Sci.*, vol. 53, no. 3, pp. 1090–1095, Jun. 2006.
- [15] A. Kuhn, S. Surti, J. S. Karp, P. S. Raby, K. S. Shah, A. E. Perkins, and G. Muehlechner, "Design of a lanthanum bromide detector for time-of-flight PET," *IEEE Trans. Nucl. Sci.*, vol. 51, no. 5, pp. 2550–2557, Oct. 2004.
- [16] D. W. Cooke, K. J. McClellan, B. L. Bennett, J. M. Roper, M. T. Whittaker, R. E. Muenchausen, and R. C. Sze, "Crystal growth and optical characterization of cerium-doped Lu_{1.8}Y_{0.2}SiO₅," *J. Appl. Phys.*, vol. 88, no. 12, pp. 7360–7362, 2000.
- [17] L. Qin, H. Li, S. Lu, D. Ding, and G. Ren, "Growth and characteristics of LYSO (Lu_{2(1-x-y)}Y_{2x}SiO₅: Ce_y) scintillation crystals," *J. Cryst. Growth*, vol. 281, no. 2–4, pp. 518–524, 2005.
- [18] M. Ito, J. S. Lee, S. Il Kwon, G. S. Lee, B. Hong, K. S. Lee, K.-S. Sim, S. J. Lee, J. T. Rhee, and S. J. Hong, "A four-layer DOI detector with a relative offset for use in an animal PET system," *IEEE Trans. Nucl. Sci.*, vol. 57, no. 3, pp. 976–981, Jun. 2010.
- [19] S. J. Hong, I. C. Song, M. Ito, S. I. Kwon, G. S. Lee, K.-S. Sim, K. S. Park, J. T. Rhee, and J. S. Lee, "An investigation into the use of geiger-mode solid-state photomultipliers for simultaneous PET and MRI acquisition," *IEEE Trans. Nucl. Sci.*, vol. 55, no. 3, pp. 882–888, Jun. 2008.
- [20] S. J. Hong, C. M. Kim, S. M. Cho, H. Woo, G. B. Ko, S. I. Kwon, J. T. Rhee, I. C. Song, and J. S. Lee, "A feasibility study on the use of optical fibers for the transfer of scintillation light to silicon photomultipliers," *IEEE Trans. Nucl. Sci.*, vol. 58, no. 3, pp. 579–589, Jun. 2011.
- [21] J. P. Lee, M. Ito, and J. S. Lee, "Evaluation of a fast photomultiplier tube for time-of-flight PET," *Biomed. Eng. Lett.*, vol. 1, no. 3, pp. 174–179, 2011.
- [22] S. J. Hong, S. Il Kwon, M. Ito, G. S. Lee, K.-S. Sim, K. S. Park, J. T. Rhee, and J. S. Lee, "Concept verification of three-layer DOI detectors for small animal PET," *IEEE Trans. Nucl. Sci.*, vol. 55, no. 3, pp. 912–917, Jun. 2008.
- [23] G. B. Ko, H. S. Yoon, S. I. Kwon, S. J. Hong, D. S. Lee, and J. S. Lee, "Development of FPGA-based coincidence units with veto function," *Biomed. Eng. Lett.*, vol. 1, no. 1, pp. 27–31, 2011.
- [24] S. I. Kwon, J. S. Lee, H. S. Yoon, M. Ito, G. B. Ko, J. Y. Choi, S.-H. Lee, I. C. Song, J. M. Jeong, D. S. Lee, and S. J. Hong, "Development of small-animal PET prototype using silicon photomultiplier (SiPM): Initial results of phantom and animal imaging studies," *J. Nucl. Med.*, vol. 52, no. 4, pp. 572–579, 2011.
- [25] V. C. Spanoudaki and C. S. Levin, "Investigating the temporal resolution limits of scintillation detection from pixelated elements: comparison between experiment and simulation," *Phys. Med. Biol.*, vol. 56, no. 3, pp. 735–756, 2011.
- [26] P. Lecoq, E. Auffray, S. Brunner, H. Hillemanns, P. Jarron, A. Knapitsch, T. Meyer, and F. Powolny, "Factors influencing time resolution of scintillators and ways to improve them," *IEEE Trans. Nucl. Sci.*, vol. 57, no. 5, pp. 2411–2416, Oct. 2010.

- [27] S. Liu, H. Li, Y. Zhang, H. Baghaei, R. Ramirez, and W.-H. Wong, "Monte Carlo simulation study on the time resolution of a PMT-quadrant-sharing LSO detector block for time-of-flight PET," *IEEE Trans. Nucl. Sci.*, vol. 56, no. 5, pp. 2614–2620, Oct. 2009.
- [28] W. W. Moses and M. Ullisch, "Factors influencing timing resolution in a commercial LSO PET camera," *IEEE Trans. Nucl. Sci.*, vol. 53, no. 1, pp. 78–85, Feb. 2006.
- [29] L. G. Hyman, "Time resolution of photomultiplier systems," *Rev. Sci. Instrum.*, vol. 36, no. 2, pp. 193–196, 1965.
- [30] T. Szczesniak, M. Moszynski, A. Nassalski, P. Lavoute, and A. G. Dehaine, "A further study of timing with LSO on XP20D0 for TOF PET," *IEEE Trans. Nucl. Sci.*, vol. 54, no. 5, pp. 1464–1473, Oct. 2007.
- [31] RoentDek Handels GmbH, The RoentDek Constant Fraction Discriminators CFD8b, CFD4b and CFD1b.
- [32] M. Aykac, F. Bauer, C. W. Williams, M. Loope, and M. Schmand, "Timing performance of Hi-Rez detector for time-of-flight (TOF) PET," *IEEE Trans. Nucl. Sci.*, vol. 53, no. 3, pp. 1084–1089, Jun. 2006.
- [33] C. Moisan, D. Vozza, and M. Loope, "Simulating the performances of an LSO based position encoding detector for PET," *IEEE Trans. Nucl. Sci.*, vol. 44, no. 6, pp. 2450–2458, Dec. 1997.
- [34] M. Moszynski, M. Kapusta, A. Nassalski, T. Szczesniak, D. Wolski, L. Eriksson, and C. L. Melcher, "New prospects for time-of-flight PET with LSO scintillators," *IEEE Trans. Nucl. Sci.*, vol. 53, no. 5, pp. 2484–2488, Oct. 2006.
- [35] T. Szczesniak, M. Moszynski, L. Swiderski, A. Nassalski, P. Lavoute, and M. Kapusta, "Fast photomultipliers for TOF PET," *IEEE Trans. Nucl. Sci.*, vol. 56, no. 1, pp. 173–181, Feb. 2009.
- [36] W. W. Moses, "Recent advances and future advances in time-of-flight PET," *Nucl. Instrum. Methods Phys. Res. A*, vol. 580, no. 2, pp. 919–924, 2007.
- [37] M. Ito, S. J. Hong, and J. S. Lee, "Positron emission tomography (PET) detectors with depth-of- interaction (DOI) capability," *Biomed. Eng. Lett.*, vol. 1, no. 2, pp. 70–81, 2011.
- [38] M. Conti, "Improving time resolution in time-of-flight PET," *Nucl. Instrum. Methods Phys. Res. A*, vol. 648, no. 1, pp. 194–198, 2011.